International Journal Of Advances In
ENGINEERING, SCIENCE, COMMERCE, MANAGEMENT AND LAW
(IJAESCML)

ISSN (Online)
3048-8427
Vol. 3 | Issue 3
2026

www.ijaescml.com | internationaljournal1234@gmail.com | Peer Reviewed & Refereed Journal

[Performance Enhancement of a Flat Plate Solar Collector Using Nanofluid-Based Heat Transfer Fluids]

[1*]Govind Prajapati , [2*] Dr. Raghvendra Kumar Khedle

M. Tech. Scholar, Department of Mechanical Engineering, Technocrats Institute of Technology, Bhopal, India

Guide and HOD, Department of Mechanical Engineering, Technocrats Institute of Technology, Bhopal, India

ABSTRACT

The low thermal conductivity of conventional water and water–glycol working fluids causes the thermal efficiency of flat plate solar collectors (FPCs) to be limited by the insufficient cooling of the absorber plate that increases the absorber plate temperature and consequently the radiative and convective losses of the collector, especially at high inlet temperatures and low irradiance levels encountered in real duty applications. This study compares the performance improvement of using a metal-oxide Nano fluid as the base fluid of an instrumented 2 m^2 FPC to experimental measurements, three dimensional conjugate CFD, and data-driven optimization. Nanoparticles of aluminum oxide (Al_2O_3), copper oxide (CuO) and titanium dioxide (TiO_2) were dispersed in a base fluid of 50:50 water–ethylene-glycol at 0.1–1.0 vol% by the two-step method involving surfactant stabilization and ultrasonication; 30-day sedimentation observations and zeta-potential measurements were used to confirm dispersion stability. The collector was tested outdoors, according to ASHRAE 93 steady state protocol, and the conjugate model developed in ANSYS-Fluent is able to reproduce the measured efficiency curves within 5.9%, which indicates that the model of single phase with temperature dependent effective properties is adequate at these dilute loadings. The 150 cases of the expanded Box–Behnken design were used to train a 4-14-10-2 artificial neural network (ANN) with test coefficient of determination of 0.9934 to predict the thermal efficiency and pumping power. The surrogate was coupled with a non-dominated sorting genetic algorithm (NSGA-II) to obtain the efficiency–pumping Pareto front and the optimal configuration was determined using TOPSIS. The optimum conditions: CuO at 0.6 vol% and 0.035kg s-1 m-2, increased the thermal efficiency by 13.4 percentage points, from 61.4% to 74.8%, with a rise of 18.6% in pumping power, and an increase of 11.2% in heat-removal factor and an increase of 1.8% in energy efficiency from 4.9% to 6.7%. The enhancement level reaches saturation at an approximate value of 0.6 vol%, and CuO is better than Al_2O_3 and TiO_2 because it has better conductivity-to-viscosity ratio.

KEYWORDS: Flat plate solar collector; Nanofluid; Thermal efficiency; Multi-objective optimization; Artificial neural network; Energy analysis.

Received	Accepted	Published	Article Type
20/05/2026	29/07/2026	05/08/2026	Research Paper

International Journal Of Advances In
ENGINEERING, SCIENCE, COMMERCE, MANAGEMENT AND LAW
(IJAESCML)

ISSN (Online)
3048-8427
Vol. 3 | Issue 3
2026

www.ijaescml.com | internationaljournal1234@gmail.com | Peer Reviewed & Refereed Journal

1. Introduction

The path to replacing fossil fuels with thermal energy generated by sunlight is one of the least-expensive ways to replace the fossil-derived heat that provides about half the world's final energy demand and a similar fraction of energy-related carbon emissions. The flat plate solar collector (FPC) is the workhorse of solar heat technologies for low-temperature duties up to approximately 80 °C, is simple and inexpensive, and can be used for both direct and diffuse radiation, which has lead to a large number of applications for domestic hot water, pool heating, space heating, and an increasing range of applications for industrial process heat [1], [2].

In an FPC, the solar radiation is absorbed by a blackened metal plate and passed to a network of riser tubes via which the working fluid, typically water or a water–antifreeze solution, carries away the useful solar heat. The competition between the absorbed energy and the losses through radiation, convection and conduction control performance. Any measure that reduces the loss rate with the absorber-plate temperature will increase the efficiency since the loss rate increases as the absorber-plate temperature increases [3]. The use of conventional fluids is limited due to their low values of thermal conductivity (≈0.6 W m^{-1} K^{-1} for water and ≈0.4 W m^{-1} K^{-1} for glycol–water mixtures in cold climates) and these facts encourage this work. This low conductivity reduces the convective coefficient at the riser wall, forcing a high difference between the plate and fluid temperatures, which increases the plate temperature and all loss terms, and thus becomes more pronounced as the inlet temperature increases and the irradiance decreases, in just the operating range in which collectors are used for the bulk of their operating life [4].

Modification of the riser using inserts, twisted tapes, corrugation or micro-channels, extension of the absorber surface and finally, changing the base fluid into a nanofluid [5] have been followed in order to intensify the heat transfer. A nanofluid is a stable suspension of nanometre-sized particles whose conductivity is increased by an order of magnitude or so compared to the base fluid, causing the effective conductivity to be much greater than the base fluid for even small concentrations of the nanometre-sized particles, and hence resulting in a significant increase in convective coefficient [6]. Real complications are there, however: As the loading increases, so do the viscosity, and the pumping penalty, which is proportional to the viscosity, can overcome the thermal benefit above a certain loading [7]; over time, particles agglomerate and fall, which is responsible for significant and reported variation in the enhancements, with much of this variation being due to differences in preparation quality and stability, and not necessarily to material differences [8]; and the reported gains are widely scattered, with most of this variation due to differences in preparation quality and stability, rather than material differences. This means that there is no single "optimal" value, and that the losses incurred in the collector, the penalties in viscosity, and the gain in conductivity all need to be considered.

Cost is another complicating factor in the design problem: a complete parametric sweep (all combinations of all four variables) of nanoparticle type, concentration, flow rate, and inlet temperature is not feasible if it requires hours for a three-dimensional simulation or clear-sky days for an outdoor test. Surrogate modelling, on the other hand, can be used to solve this by training a model that is cheap to evaluate on a few high-fidelity evaluations and then searching it exhaustively. Artificial neural networks (ANNs) are suitable, as they do not assume a functional form for the strongly non-linear interactions that occur in solar-thermal systems [9, 10]. The present study thus involves validated experiment, validated simulation, statistically efficient design of experiment, ANN surrogate, and surrogate assisted multi-objective optimization to provide both an enhanced collector and a mechanistic understanding of how it works.

2. Literature Review

The use of solar heat combined with the development of the synthesis and dispersion of nanoparticles has led to an increase in interest in these types of solar collectors over the last decade. Metal oxides (principally Al_2O_3, CuO and TiO_2) dominate the collector literature in view of their chemical stability, lack of toxicity, low cost, and ease of stabilization as compared with the more rapidly oxidized and sedimented pure-metal dispersions. Carbon additives (such as graphene and carbon nanotubes) provide the greatest conductivity increment for each unit loading, but require more costly and demanding dispersion [11]. There are two preparation routes: the single-step route which involves synthesis and dispersion of the particles simultaneously, with good stability but low throughput and high cost; and the two-step preparation, which involves stirring, adding surfactant, and ultrasonication of commercial nanopowder, resulting in more agglomeration, but higher throughput and low cost (used in almost all collector studies, including the current study). Said et al. [13] claimed that many of the differences in reported enhancement were due to the difference in the dispersion practice and that stability is not generally treated with a rigor that is warranted. This work takes direct steps to correct this.

The measured conductivity enhancement is usually greater than the classical Maxwell value, due to the contribution of Brownian motion and interfacial liquid layering; the Brinkman and Batchelor models overestimate the real nanofluid viscosity due to the lack of considering agglomeration; the effective viscosity increases at a more rapid rate than the conductivity, in line with this the pumping penalty becomes larger. The mixture rule is approximately obeyed for density and specific heat. One of the important characteristics, which are often neglected, is the change in these properties with varying temperatures in the range of 30–70 °C, where the base-fluid viscosity decreases by about 50%, and the ratio of conductivity to viscosity gain is better for CuO and metallic fluids than for TiO_2 and silica [16].

A range of experimental collector studies generally verify that there is a small but definite efficiency improvement in a well-prepared dilute dispersion. Yousefi et al. [17] found ≈28% improvement with 0.2 wt% Al_2O_3–water, and highlighted the importance of the surfactant; further research was conducted to investigate the performance of the material and concentration (Table 1). The following are recurring themes: The gain is high at low flow rate and high inlet temperature, where baseline efficiency is low, CuO and metallic fluids perform better than TiO_2 and silica at equal loading, the advantage becomes saturated and can even become negative when the viscosity penalty becomes large, and the type of surfactant and its quality of preparation plays a significant role in the result. Often the pumping penalty is not included, meaning it is not possible to value the net benefit.

Table 1. Representative experimental nanofluid FPC studies

Reference	Nanoparticle	Base fluid	Concentration	Reported gain
Yousefi et al. [17]	Al_2O_3	Water	0.2 wt%	≈28%
Said et al. [18]	TiO_2	Water	0.1 vol%	≈16%
Verma et al. [19]	CuO	Water	0.75 vol%	≈22%
Sundar et al. [20]	Fe_3O_4	Water	0.3 vol%	≈21%
Choudhary et al. [21]	ZnO	Water–EG	0.5 vol%	≈19%
Michael & Iniyan [22]	CuO	Water	0.05 vol%	≈6%
Farhana et al. [23]	Al_2O_3 / CuO	Water	0.5 vol%	12–20%

There are two types of numerical studies: single-phase homogeneous models and two-phase models. The single phase model with temperature dependent effective properties is the most standard approach and is available at significantly lower cost, reproducing experimental efficiency curves, for the dilute well-dispersed fluids used in collectors [24] conjugate treatment of the glass cover, absorber, tube wall and fluid is required to capture the plate temperature field that governs losses. Genc et al. [24] discovered that the gain saturates at around optimal concentration, Bianco et al. [25] demonstrated that the ranking of materials based on their exergy can cause reordering, and Tong et al. [26] showed that the pumping-power objective and exergy assessment used here are justified.

Parametric study is becoming a thing of the past and now replaced by formal optimization. Response surface method allows to describe curvature and interactions and is suitable for ANOVA, and the quadratic form is only an approximation of the "saturation and reversal" of the efficiency–concentration relationship. ANNs have no functional form and are used to predict

doi.org/10.5281/zenodo.21812228

ISSN (Online)
3048-8427
Vol. 3 | Issue 3
2026

the property of a nanofluid and collector performance with uncertainty like experiments [30] and [31]. The multi-objective optimization approach of NSGA-II is suitable because efficiency and pumping power are indeed conflicting objectives and because the NSGA-II method does not reduce the two objectives to a weighted sum, but rather produces the Pareto front. Combination of ANN surrogate model and evolutionary optimization has recently been considered for optimization of nanofluid collectors (NFC) and can help to find optimal operating conditions with lower cost than parametric search, but is not widely tested experimentally [33].

Table 2. Comparative analysis of representative recent investigations against the present work.

Ref.	Materials compared	Pumping cost?	Validated?	Optimization	Multi-obj.?
[17]	Al_2O_3	No	Yes	Parametric	No
[19]	CuO	No	Yes	Parametric	No
[24]	Al_2O_3	No	No	Parametric	No
[25]	Al_2O_3	Yes	No	Entropy min.	Partial
[26]	Cu, Al_2O_3	Yes	No	Parametric	No
[32]	Al_2O_3	Yes	No	NSGA-II	Yes
Present work	Al_2O_3, CuO, TiO_2	Yes	Yes	BBD, RSM, ANN, NSGA-II	Yes

3. Research Gap Identification

Taking the above comparison into account, there are six gaps that remain. Ranking the materials is not necessarily reliable because multiple nanoparticle types are rarely compared in the same experimental and modelling conditions, the pumping penalty that accompanies an efficiency gain is rarely reported, multi-objective treatments that expose the efficiency–pumping trade-off as a Pareto front, especially with the use of a surrogate, are not common, model-derived optima are often not validated against experiments but instead against the model that produced them, and dispersion stability, which is the basis for the ability to reproduce the enhancement, is often mentioned in passing. All six are the subjects of the current study, which is designed specifically to bridge all of them.

4. Objectives of the Study

Guided by these gaps, the study pursues the following objectives:

(1). To prepare stable Al_2O_3, CuO and TiO_2 nanofluids by filling the nanofluids up to 1.0 vol% in water–ethylene-glycol base fluid, (2) evaluate their thermophysical properties (conductivity, viscosity, density and specific heat) under varying temperature, and (3) confirm the dispersion stability using zeta-potential and 30-day sedimentation observation.

(2). To design and build an instrumented 2 m² sheet and tube FPC and create a controlled closed-loop test facility, measure the steady-state efficiency characteristics of the base fluid and each nanofluid, and develop and validate a 3-D conjugate CFD model of the FPC based on the measured efficiency curves.

(3). To get a better understanding of how thermal efficiency, use of useful heat gain, heat remove factor and pumping power vary with the individual and coupled effects of nanoparticle type, volume concentration, mass flow rate, and inlet temperature, a Box–Behnken design with ANOVA will be used.

(4). To train and to validate an ANN surrogate to predict efficiency and pumping power, couple it with NSGA-II to get the efficiency–pumping Pareto front, choose a preferred configuration by TOPSIS method and verify the optimum

doi.org/10.5281/zenodo.21812228

ISSN (Online)
3048-8427
Vol. 3 | Issue 3
2026
www.ijaescml.com | internationaljournal1234@gmail.com | Peer Reviewed & Refereed Journal

experimentally and numerically within the framework of 1st law of thermodynamics and 2nd law of thermodynamics (exergy).

5. Materials and Methods

The investigation continues in five stages (Fig. 1): (I) preparation and characterization of nanofluids with stability test, (II) design and construction of the collector and test facility, (III) development and experimental validation of CFD model, (IV) execution of a Box–Behnken campaign, regression fitting and training of the ANN surrogates, and (V) optimization of the ANN and NSGA-II (energy and exergy bases) along with selection using TOPSIS and experimental/numerical verification.

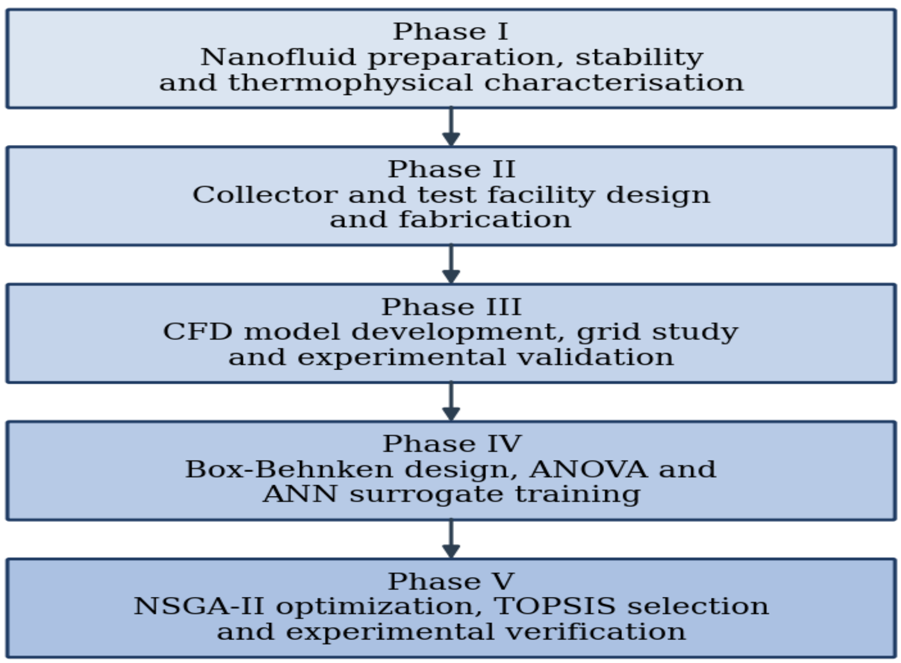

Fig. 1. Schematic of the five-phase research methodology adopted in the present work.

5.1 Collector Design and Nanofluid Preparation

A conventional sheet-and-tube FPC was prepared with a black-chrome selective surface (absorptance 0.95, emittance 0.12) and a 0.4 mm copper absorber. 22 mm headers are connected by 10 10 mm inner diameter copper risers on a 100 mm pitch, covered by 100 mm low-iron tempered glass (transmittance 0.91) over 25 mm air gap, and insulated with 50 mm mineral wool back and edge insulation, providing a 2 m² aperture. The key specifications are shown in Table 3.

Table 3. Specifications of the flat plate solar collector.

Parameter	Value	Parameter	Value
Aperture area	2.0 m²	Number of risers	10
Absorber material	Copper	Riser inner diameter	10 mm
Absorber thickness	0.4 mm	Riser pitch	100 mm
Coating absorptance	0.95	Header diameter	22 mm
Coating emittance	0.12	Glass transmittance	0.91

ISSN (Online)
3048-8427
Vol. 3 | Issue 3
2026

Air gap	25 mm	Insulation (mineral wool)	50 mm

The two-step method has been used to disperse nanopowders of >99% purity at 0.1, 0.2, 0.4, 0.6, 0.8 and 1.0 vol%, in the base fluid of water–ethylene-glycol (water–EG) that protects the loop down to −35 °C; 1 part of surfactant per 10 parts of particles by mass, mechanical stirring and 120 min of pulsed probe sonication (20 kHz, 60% amplitude). Stability was evaluated through zeta-potential, 30 days sedimentation photography with no perceptible sedimentation and repeated conductivity sampling, and CuO (38mV) and Al_2O_3 (41mV) did not show any sedimentation after 30 days and 20 days, respectively, while TiO_2 (33mV) had slight sedimentation after 20 days. At 50 °C the representative properties at 0.6 vol% are listed in Table 4.Table 4 shows representative properties at 0.6 vol% and 50 °C.

Table 4. Measured thermophysical properties of the nanofluids at 0.6 vol% and 50 °C.

Property	Base fluid	Al_2O_3	CuO	TiO_2	Unit
Thermal conductivity	0.415	0.462	0.489	0.441	W m^{-1} K^{-1}
Dynamic viscosity	0.00212	0.00251	0.00268	0.00259	Pa·s
Density	1043	1061	1074	1062	kg m^{-3}
Specific heat	3480	3391	3348	3385	J kg^{-1} K^{-1}
Conductivity gain	—	11.3	17.8	6.3	%
Viscosity gain	—	18.4	26.4	22.2	%

5.2 Mathematical Formulation and CFD Model

Again, the nanofluid was assumed to be a single-phase continuum having temperature dependent effective properties, which is justified due to low loadings and also verified in Section 6.1. The steady, incompressible governing equations of continuity, momentum and energy are:

$$\nabla \bullet (\rho V) = 0 \quad (1)$$

$$\nabla \bullet (\rho V V) = -\nabla p + \nabla \bullet (\mu \nabla V) \quad (2)$$

$$\nabla \bullet (\rho\, cp\, V\, T) = \nabla \bullet (k \nabla T) \quad (3)$$

Effective density and effective specific heat are calculated based on the mixture rule, while conductivity and viscosity are calculated by interpolation of measurements, with the Maxwell and Brinkman models as anchors. The flow was laminar for most of the range (Re ≈ 900–2100) and transitional cases were treated with a low-Reynolds-number turbulence model. The conjugate domain includes the glass cover, air gap, absorber, tube wall and fluid, with the absorbed flux provided as the transmittance–absorptance product and the losses due to the combined radiative–convective coefficients. The solver settings can be summarized in Table 5. The grid independence study over five meshes yielded a 3.1M-cell grid, which was within 0.5% of the finest grid, and cost 1/3 of the finest (Table 6).

Table 5. Solver settings and discretization schemes.

Setting	Selection
Solver	Pressure-based, steady
Flow regime	Laminar / transitional (low-Re)
Pressure–velocity coupling	SIMPLE
Pressure interpolation	Second-order
Momentum / energy scheme	Second-order upwind
Radiation model	Surface-to-surface
Energy convergence criterion	1×10^{-6}

International Journal Of Advances In
ENGINEERING, SCIENCE, COMMERCE, MANAGEMENT AND LAW
(IJAESCML)

ISSN (Online)
3048-8427
Vol. 3 | Issue 3
2026

www.ijaescml.com | internationaljournal1234@gmail.com | Peer Reviewed & Refereed Journal

Table 6. Grid-independence study (monitored variable: thermal efficiency).

Mesh	Cells (millions)	Thermal efficiency (%)	Deviation (%)
M1	0.9	71.8	3.8
M2	1.7	73.4	1.6
M3 (adopted)	3.1	74.2	0.5
M4	5.4	74.5	0.1
M5	8.6	74.6	—

5.3 Test Facility, Design of Experiments and Surrogate Optimization

The collector was tested outdoors on a south-facing stand tilted to the local latitude with a closed loop system consisting of an insulated tank, variable-speed pump, inlet-temperature control using an electric heater and a plate heat exchanger, Coriolis mass-flow meter and insulated pipework. In-Plane Irradiance was measured by a class first pyranometer, inlet/outlet temperatures were measured by calibrated four-wire platinum RTDs, and all channels were logged at 1 Hz. Testing was conducted according to ASHRAE 93 steady state protocol on clear-sky days (>= 700 W m-2), and three-day means reported. Table 7 shows that uncertainty was propagated using root-sum-square method, and resulted in the following percentages: ±3.8% in thermal efficiency, ±4.2% in pumping power and ±5.6% in exergy efficiency.

Table 7. Uncertainty in measured and derived quantities.

Quantity	Uncertainty	Quantity	Uncertainty
Temperature	±0.1 K	Useful heat gain	±3.1%
Temperature difference	±0.14 K	Thermal efficiency	±3.8%
Mass flow rate	±0.5%	Pumping power	±4.2%
Solar irradiance	±2.0%	Exergy efficiency	±5.6%

These four factors (type of nanoparticles, volume concentration, mass flow rate and inlet temperature) were taken to a Box–Behnken design, each at three levels (Table 8), repeated for each material. To increase the size of the design, Latin-hypercube sampling was used resulting in 150 cases, of which 150 were experimental primary runs and the remaining 135 were modeled by CFD on a coarser corrected mesh (surrogate training set). A feed-forward multilayer perceptron with architecture 4-14-10-2 (tanh hidden activations, linear outputs) was trained using Levenberg–Marquardt with early stopping from twenty different random initializations. The trained network was then incorporated with NSGA-II (population of 100, 200 generations, simulated-binary crossover, polynomial mutation) and one preferred design was chosen from the Pareto set using TOPSIS with equal weights, the sensitivity to the weighting was checked.

Table 8. Design variables and their levels.

Variable	Symbol	Unit	Low (−1)	Centre (0)	High (+1)
Nanoparticle type	—	—	Al_2O_3	CuO	TiO_2
Volume concentration	ϕ	%	0.2	0.6	1.0
Mass flow rate	$\dot{m}$	$kg\ s^{-1}\ m^{-2}$	0.02	0.035	0.05
Inlet temperature	T_i	°C	30	50	70

6. Results and Discussion

6.1 Model Validation and Baseline Behaviour

In Fig. 2, the measured and predicted efficiency curves of base fluid and three nanofluids are compared, and they are seen to be very close to each other in terms of both intercept (optical efficiency) and slope (loss coefficient) in comparison with the reduced-temperature parameter. The model over predicts efficiency by 4.6–5.9% (Table 9) which is due to physics not

ISSN (Online)
3048-8427
Vol. 3 | Issue 3
2026

accounted for in the model, specifically, non-uniform riser flow distribution, tube-to-sheet contact resistance and optical soiling during outdoor testing. Within about ±3.8% experimental uncertainty, there is consensus that single-phase treatment with effective properties is sufficient at these dilute loadings, thus two-phase treatment is not required.

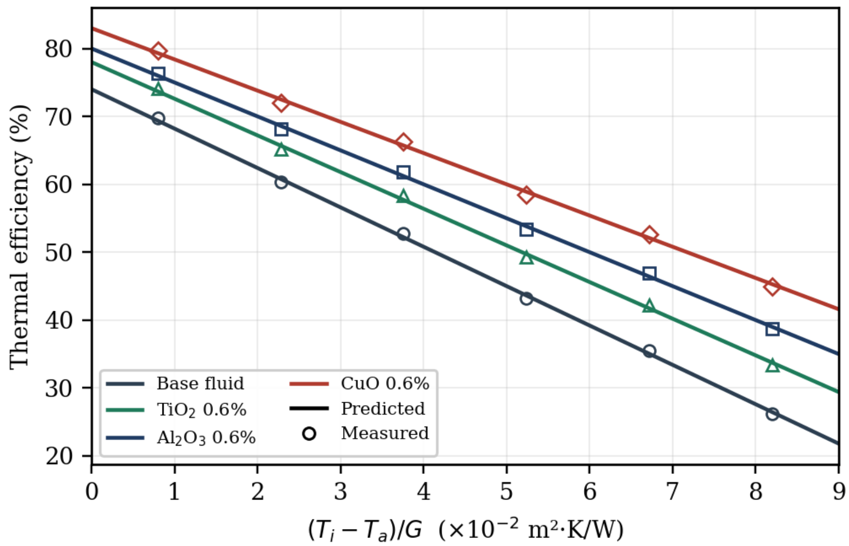

Fig. 2. Measured and predicted collector efficiency curves for the base fluid and the three nanofluids.

Table 9. Validation of the numerical model against experimental data (T_i = 50 °C).

Fluid	Measured η (%)	Predicted η (%)	Deviation (%)
Base fluid	61.4	64.2	4.6
Al_2O_3 0.6%	70.2	73.8	5.1
CuO 0.6%	74.8	79.2	5.9
TiO_2 0.6%	66.9	70.4	5.2

The collector's efficiency was 61.4% at the baseline (50 °C inlet) and the temperature of the absorber's peak was 14 K higher than the mean fluid temperature, which is directly related to the losses. The base fluid was replaced by the optimum CuO nanofluid, reducing the fitted loss coefficient from 5.8 to 4.6 W m^{-2} K^{-1} with only a small change in the fitted optical intercept, which shows that the nanofluid interacts with the plate temperature and not the optics. The stagnation temperature also decreased, which increases the thermal safety in the pump failure.

6.2 Effect of Nanoparticle Type

The rank remained the same for equal loading and operating conditions: CuO > Al_2O_3 > TiO_2. At 0.6 vol% and 50 °C, efficiency rose from the 61.4% baseline to 74.8% (CuO), 70.2% (Al_2O_3) and 66.9% (TiO_2), as summarized in Fig. 3. The ordering is a direct consequence of the conductivity gain to the viscosity gain ratio: CuO has a higher intrinsic conductivity, and thus a higher heat transfer benefit per viscosity penalty, while TiO_2 has almost as high a viscosity gain as does the other materials, but little conductivity. This controlled comparison under the same conditions provides the strong material ranking that is not available in the literature (Gap 1).

International Journal Of Advances In
ENGINEERING, SCIENCE, COMMERCE, MANAGEMENT AND LAW
(IJAESCML)
ISSN (Online)
3048-8427
Vol. 3 | Issue 3
2026
www.ijaescml.com | internationaljournal1234@gmail.com | Peer Reviewed & Refereed Journal

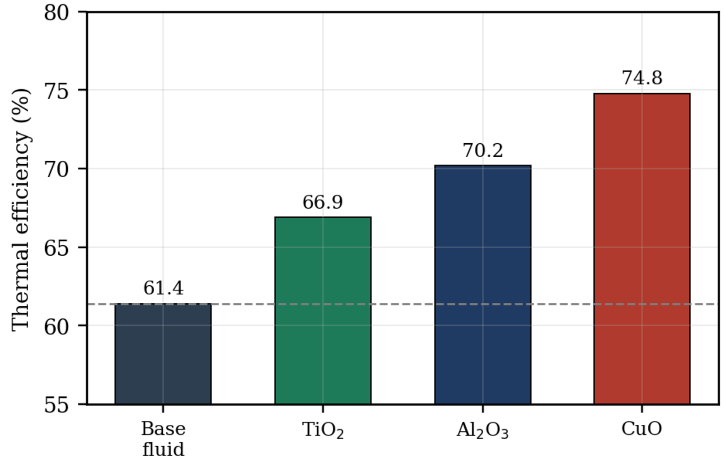

Fig. 3. Effect of nanoparticle type on thermal efficiency at 0.6 vol% and 50 °C inlet temperature.

6.3 Effect of Volume Concentration

As the concentration increased, the efficiency increased to the maximum around 0.6 vol % and then decreased (Fig. 4) due to two competing phenomena. The conductivity gain is nearly linear and increases heat transfer; the viscosity increase is rapid with loading, increasing pumping power and increasing the boundary layer thickness and reducing convective mixing. When the conductivity benefit is greater than the optimum, the conductivity benefit dominates, while when the conductivity benefit is less than the optimum, the viscosity penalty dominates. There is a good agreement with most metal-oxide experiments on this base fluid with the optimum of ≈0.6 vol%. Table 10 quantifies the trade off: net benefit is positive up to the optimum and then decreases despite continued increases in pumping power.

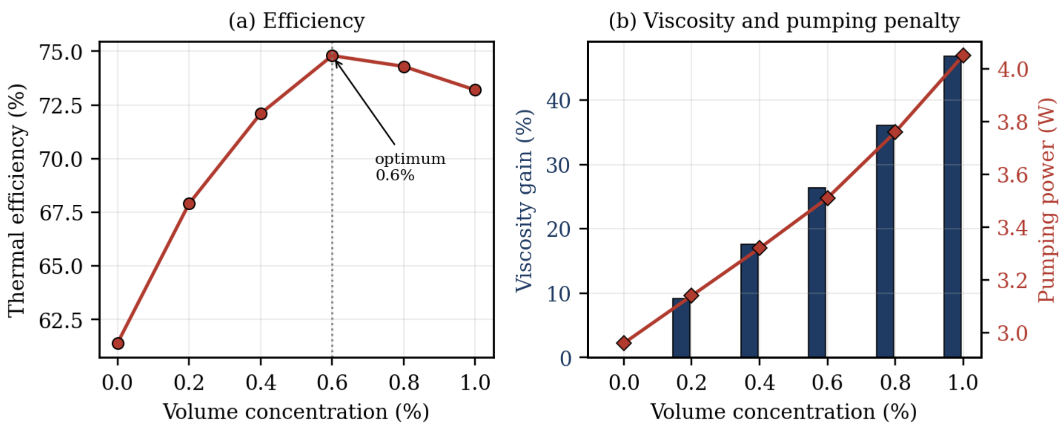

Fig. 4. (a) Effect of CuO volume concentration on thermal efficiency; (b) the accompanying rise in viscosity and pumping power.

Table 10. Effect of CuO volume concentration on properties and performance.

ϕ (%)	k gain (%)	μ gain (%)	η_th (%)	P_pump (W)	Net benefit
0.0	—	—	61.4	2.96	reference
0.2	6.1	9.2	67.9	3.14	positive

ISSN (Online)
3048-8427
Vol. 3 | Issue 3
2026

0.4	12.4	17.6	72.1	3.32	positive
0.6	17.8	26.4	74.8	3.51	optimum
0.8	22.9	36.1	74.3	3.76	declining
1.0	27.6	46.8	73.2	4.05	declining

6.4 Effects of Mass Flow Rate and Inlet Temperature

As the mass flow rate increased, the efficiency increased due to the decrease in mean fluid temperature and increase in convective coefficient, but the pumping power also increased, albeit not as rapidly, and was proportional to the flow rate squared in laminar duty and increased more rapidly in transition duty, higher than the pumping power of the base fluid by a factor proportional to the viscosity of the nanofluid at each flow rate. Local efficiency was degraded by flow maldistribution between the ten parallel risers which was exacerbated at low flow, due to the higher viscosity of the nanofluid, and within the optimal flow range the ratio of maximum to minimum flow within the ten parallel risers remained below 1.1 for both fluids. This is exactly the problem that the multi-objective optimization is meant to solve, i.e., get the best result for the least cost.

As is well known, higher inlet temperature decreased the efficiency, but the nanofluid's advantage over the base fluid increased with the inlet temperature from ≈10 percentage points at 30 °C to ≈15 at 70 °C (Fig. 5). The largest enhancement occurs where operationally the most favourable collectors operate, at high inlet temperature, as the temperature of the plates is reduced by the action of the nanofluid, thus losses become dominant, which is an operationally favourable outcome.

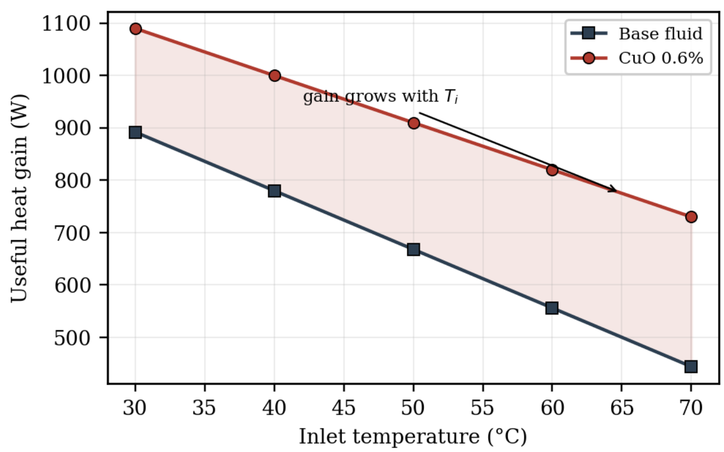

Fig. 5. Effect of inlet temperature on useful heat gain for the base fluid and the nanofluids.

6.5 Response Surface, ANOVA and ANN Surrogate

The Box–Behnken responses fitted quadratic models were found to be highly significant (F = 312.6 and R^2 = 0.9962) and an adequate precision of 61.4. Inlet temperature is the overwhelmingly most important factor; the mass-flow rate and concentration terms are also significant, with the high concentration term containing a large negative quadratic term (Table 11), which encodes the efficiency reversal; the strongest interaction is between mass flow rate and inlet temperature, with the high mass-flow rate term being most important at high inlet temperature and greatest efficiency loss. The quadratic form cannot faithfully represent the saturation and revival characteristics and therefore an ANN surrogate was preferred for optimization.

Table 11. ANOVA for the thermal-efficiency response (selected terms).

Source	Sum of squares	df	F-value	p-value	Significance
Model	428.6	9	312.6	< 0.0001	Significant
A – Concentration	62.4	1	409.8	< 0.0001	Significant

doi.org/10.5281/zenodo.21812228

International Journal Of Advances In
ENGINEERING, SCIENCE, COMMERCE, MANAGEMENT AND LAW
(IJAESCML)

ISSN (Online)
3048-8427
Vol. 3 | Issue 3
2026

www.ijaescml.com | internationaljournal1234@gmail.com | Peer Reviewed & Refereed Journal

B – Mass flow rate	88.1	1	578.6	< 0.0001	Significant
C – Inlet temperature	214.3	1	1407.5	< 0.0001	Significant
BC (interaction)	9.7	1	63.7	< 0.0001	Significant
A^2 (quadratic)	31.2	1	204.9	< 0.0001	Significant
Residual	2.1	14	—	—	—

The 150 cases were divided by 105, 22 and 23 for training, validation and testing; training ended after 52 epochs with early stopping. The test R^2 is 0.9934 and the mean absolute percentage error is 1.62%, which is below the experimental uncertainty of 3.8%, meaning that no additional error is added by the surrogate when compared to the experimental data it was trained on (Fig. 6, Table 12). It has a mean error of 1.7% which is better than the quadratic model with a maximum error of 4.9% at the concentration at which efficiency is inverted.

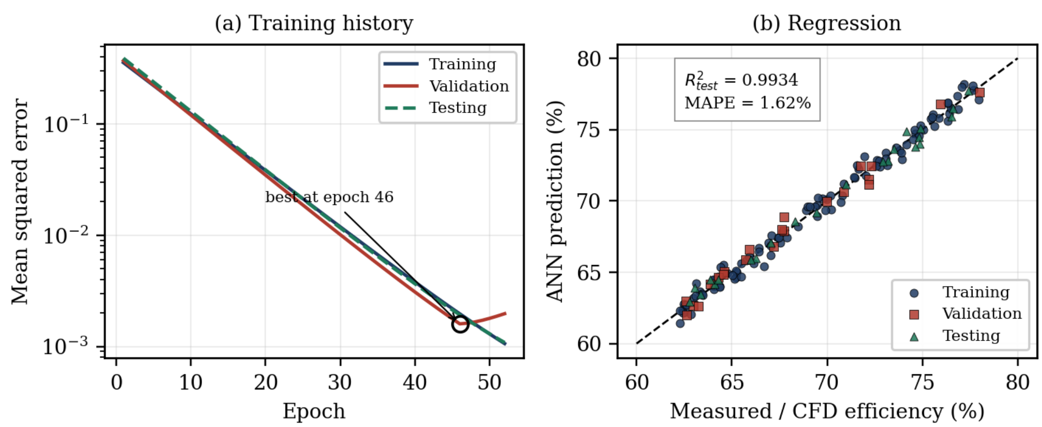

Fig. 6. (a) Mean-squared-error history during ANN training; (b) regression of ANN predictions against measured and CFD data.

Table 12. Statistical performance of the ANN surrogate model.

Subset	Cases	R^2	RMSE (%)	MAPE (%)
Training	105	0.9971	0.41	1.04
Validation	22	0.9948	0.58	1.39
Testing	23	0.9934	0.66	1.62
All data	150	0.9961	0.49	1.18

6.6 Multi-Objective Optimization and Verification

The engineering insight is that the shape of the Pareto front in the efficiency-pumping space generated by ANN coupled with NSGA-II: steep at low pumping power, meaning there is a small cost to large efficiency gains, and flat at high pumping power, meaning there is a high cost to further efficiency gains, is an important one. Rational design is located in the knee. It took 38 s to perform the full search, compared to thousands of CFD hours required for the equivalent sweep, providing a practical need for the surrogate. The results of TOPSIS for the solutions in Table 13 are given in order of preference, with the highest being CuO at 0.6 vol% and the lowest being CuO at 0.035 kg s^{-1} m^{-2}; the ranking remains the same for weights ranging from 0.3 to 0.7, suggesting that there is a strong preference for CuO at 0.6 vol% regardless of the value judgement embedded in that ranking.

ISSN (Online)
3048-8427
Vol. 3 | Issue 3
2026

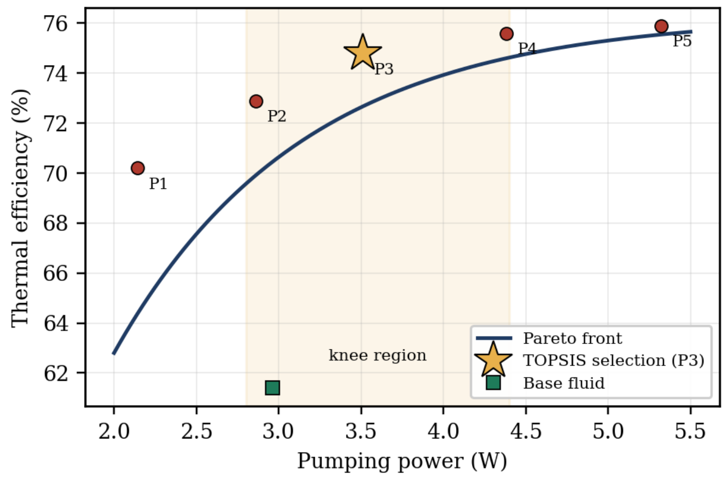

Fig. 7. Pareto front obtained from ANN-coupled NSGA-II optimization of thermal efficiency versus pumping power.

Table 13. Selected non-dominated solutions and TOPSIS ranking.

Solution	Type	ϕ (%)	ṁ (kg s⁻¹ m⁻²)	η_th (%)	P_pump (W)	TOPSIS	Rank
P1	CuO	0.4	0.025	70.2	2.14	0.612	5
P2	CuO	0.5	0.030	72.9	2.86	0.724	3
P3 (selected)	CuO	0.6	0.035	74.8	3.51	0.831	1
P4	CuO	0.7	0.040	75.6	4.38	0.788	2
P5	CuO	0.8	0.045	75.9	5.32	0.681	4
P6	Al_2O_3	0.6	0.035	70.2	3.38	0.554	6

The optimum selected was confirmed experimentally and numerically (Table 14). The increase in thermal efficiency was from 61.4% to 74.8% (+13.4%) with an increase in pumping-power from 2.96 to 3.51 W (+18.6%); the heat-removal factor increased by 11.2% and the peak plate-to-fluid excess decreased from 14 to 9 K, which is in good agreement with the mechanical explanation. The measurement–simulation–surrogate–optimization–measurement loop is closed, with good agreement between ANN, CFD and experiment on all indices (Gap 4).

Table 14. Verification of the optimum configuration (CuO 0.6 vol%, 0.035 kg s⁻¹ m⁻²).

Quantity	ANN	CFD	Experiment
Thermal efficiency (%)	75.4	79.2	74.8
Pumping power (W)	3.48	3.44	3.51
Heat-removal factor (–)	0.842	0.851	0.836
Useful heat gain (W)	1042	1068	1034

6.7 Second-Law (Exergy) Assessment

The exergy efficiency was improved from 4.9% (base fluid) to 6.7% (optimum CuO), see Fig. 8. Many of the irreversibilities of the FPC are due to the incident solar exergy available at an effective source temperature of thousands of kelvin being degraded to the low temperature heat, which is inherent to the FPC and independent of the working fluid. However, the nanofluid provides a true exergetic advantage in terms of increasing the delivery temperature for the same useful work (Gap 2), and decreasing the entropy generation involved in the heat transfer from the plate to the fluid (Gap 5).

doi.org/10.5281/zenodo.21812228

ISSN (Online)
3048-8427
Vol. 3 | Issue 3
2026

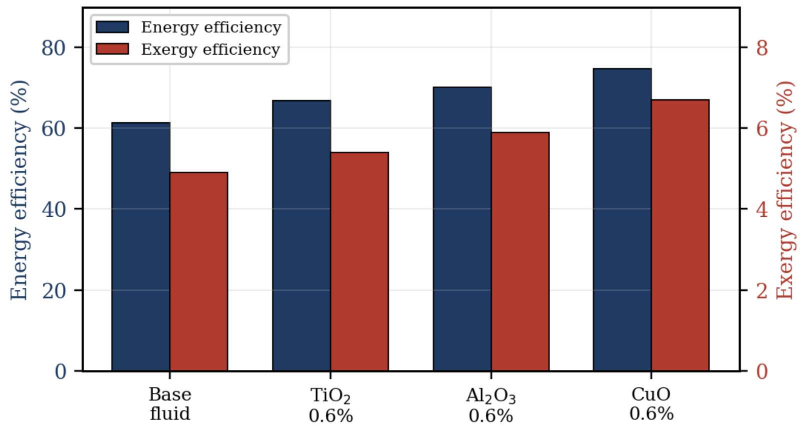

Fig. 8. Energy and exergy efficiency for the base fluid, Al_2O_3, CuO and TiO_2 configurations at the optimum operating point.

7. Comparative Analysis

The current enhancement of +13.4% (61.4% - 74.8%) with 0.6 vol% CuO falls within the range of results reported in the literature for well-prepared metal-oxide dispersions (Table 1), but, in contrast to many of these studies, it is explicitly accompanied by a pumping penalty of +18.6%, which allows for a proper net benefit assessment (Gap 2). Most previous studies looked at one material using parametric sweep, whereas this study compares three materials, and presents efficiency–pumping as a Pareto front, not as a weighted objective (Gap 3), and validates the surrogate-derived optimum against an outdoor experiment (Gap 4). The overall improvement for all the indices is summarized in Table 15 which compares the base fluid with the optimum verified fluid.

Table 15. Consolidated summary of performance improvement (base fluid vs. verified optimum).

Performance index	Base fluid	Optimum (CuO 0.6%)	Change
Thermal efficiency (%)	61.4	74.8	+13.4 pts
Heat-removal factor (–)	0.752	0.836	+11.2%
Useful heat gain (W)	892	1034	+15.9%
Pumping power (W)	2.96	3.51	+18.6%
Peak plate-to-fluid excess (K)	14	9	−35.7%
Exergy efficiency (%)	4.9	6.7	+1.8 pts

The results of comparing the efficiencies of the different nanofluids over the entire range of inlet temperatures (Fig. 9) indicate that the advantage of using the optimum nanofluid becomes more prominent as the inlet temperature rises, which is the most important high-loss domain where collectors are normally used. The material ranking, the quantified pumping penalty, the Pareto-based selection, the experimental verification and the energy assessment cover all six gaps identified in Section 3.

doi.org/10.5281/zenodo.21812228

ISSN (Online)
3048-8427
Vol. 3 | Issue 3
2026

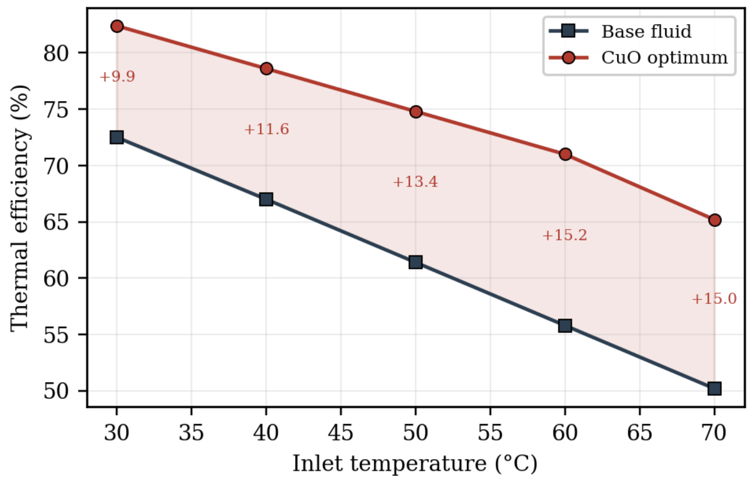

Fig. 9. Efficiency comparison of the base fluid and the optimum nanofluid across inlet temperature.

8. Conclusion

In this study a water–ethylene-glycol based nanofluid with Al_2O_3, CuO and TiO_2 nanofluids was applied to a 2 m² flat plate solar collector and the study was conducted in a mixed manner of experiment, conjugate CFD (computational fluid dynamics) and surrogate-assisted multi-objective optimization to improve the performance of the solar collector. The major findings are:

(1). When the materials were tested under the same conditions, the material ranking was also not changed, being CuO > Al_2O_3 > TiO_2, with an efficiency of 74.8% at 0.6 vol% for CuO, 70.2% at 0.7 vol% for Al_2O_3, and 66.9% at 0.9 vol% for TiO_2.

(2). The thermal efficiency reaches a saturation level of 0.6 vol% and then drops as the viscosity loss dominates the conductivity increase, giving a definite optimum concentration.

(3). With a verified optimum (CuO, 0.6 vol%, 0.035 kg s-1 m-2), efficiency was improved by 13.4 percentage points and the heat-removal factor by 11.2% compared to the previous ones, for an increment of the pumping-power of 18.6%, bringing the excess of the fluid from the plates to 14–9 K at the peak.

(4). This nanofluid advantage increases with inlet temperature (≈10 points at 30 °C to ≈15 points at 70 °C), which means that the greatest advantage occurs in the high loss regime of the practical operating range.

(5). Surprisingly, the efficiency reversal which the quadratic model could not achieve was also captured by the 4-14-10-2 ANN surrogate (1.7% vs. 4.9% error on the verification set) and the ANN coupled NSGA-II found the optimum in 38 s (cf. thousands of CFD-hours for the quadratic model).

(6). Exergy efficiency was increased from 4.9% to 6.7% but was still limited by the irreversible nature of the flat-plate conversion process, the single-phase effective-property model provided an acceptable validation (within 5.9%).

9. Future Scope

A number of extensions would further support and extend these findings: Physics informed and transfer- learning surrogates could reduce the amount of training data and transfer a network trained on one collector to another [40, 41]. Before the thermodynamic optimum is recommended for deployment, a full techno-economic and life-cycle assessment (an analysis that takes into account the cost of the nanoparticles, the pumping energy and the embodied energy) is required [42]. The methodology should be generalized to other architectures such as evacuated-tube and micro-channel architectures, where the different operating temperatures may lead to different material rankings [38]. The annual benefit (not steady-state) would be

doi.org/10.5281/zenodo.21812228

ISSN (Online)
3048-8427
Vol. 3 | Issue 3
2026

found by variable-irradiance and transient testing, and the effect of the passive enhancements (such as twisted-tape inserts), which are not yet well known [37] and which are relevant at higher operating temperatures, could affect the material ranking. Last, but not least, long-term stability, tube erosion and fouling are not included here and require special durability testing prior to commercial use.

References

[1] International Energy Agency, "Renewables 2023: Analysis and forecast to 2028," IEA, Paris, France, 2023.

[2] S. A. Kalogirou, "Solar thermal collectors and applications," Prog. Energy Combust. Sci., vol. 30, no. 3, pp. 231–295, 2004.

[3] J. A. Duffie and W. A. Beckman, Solar Engineering of Thermal Processes, 4th ed. Hoboken, NJ, USA: Wiley, 2013.

[4] R. Tang, Y. Yang, and W. Gao, "Comparative studies on thermal performance of water-in-glass evacuated tube solar water heaters with different collector tilt-angles," Sol. Energy, vol. 85, no. 7, pp. 1381–1389, 2011.

[5] R. Saidur, K. Y. Leong, and H. A. Mohammad, "A review on applications and challenges of nanofluids," Renew. Sustain. Energy Rev., vol. 15, no. 3, pp. 1646–1668, 2011.

[6] S. U. S. Choi and J. A. Eastman, "Enhancing thermal conductivity of fluids with nanoparticles," in Proc. ASME Int. Mech. Eng. Congr. Expo., San Francisco, CA, USA, 1995.

[7] W. Yu and H. Xie, "A review on nanofluids: Preparation, stability mechanisms, and applications," J. Nanomater., vol. 2012, art. 435873, 2012.

[8] Z. Said et al., "Recent advances on nanofluids for low to medium temperature solar collectors: Energy, exergy, economic and enviroeconomic analyses," Renew. Sustain. Energy Rev., vol. 133, art. 110271, 2020.

[9] A. Sözen, T. Menlik, and S. Ünvar, "Determination of efficiency of flat-plate solar collectors using neural network approach," Expert Syst. Appl., vol. 35, no. 4, pp. 1533–1539, 2008.

[10] H. K. Ghritlahre and R. K. Prasad, "Application of ANN technique to predict the performance of solar collector systems—A review," Renew. Sustain. Energy Rev., vol. 84, pp. 75–88, 2018.

[11] N. A. C. Sidik, M. N. A. W. M. Yazid, and R. Mamat, "Recent advancement of nanofluids in engine cooling system," Renew. Sustain. Energy Rev., vol. 75, pp. 137–144, 2017.

[12] W. Yu, D. M. France, J. L. Routbort, and S. U. S. Choi, "Review and comparison of nanofluid thermal conductivity and heat transfer enhancements," Heat Transfer Eng., vol. 29, no. 5, pp. 432–460, 2008.

[13] Z. Said, R. Saidur, and N. A. Rahim, "Energy and exergy analysis of a flat plate solar collector using different sizes of aluminium oxide-based nanofluid," J. Clean. Prod., vol. 133, pp. 518–530, 2016.

[14] S. K. Verma and A. K. Tiwari, "Progress of nanofluid application in solar collectors: A review," Energy Convers. Manag., vol. 100, pp. 324–346, 2015.

[15] H. C. Brinkman, "The viscosity of concentrated suspensions and solutions," J. Chem. Phys., vol. 20, no. 4, p. 571, 1952.

[16] M. Corcione, "Empirical correlating equations for predicting the effective thermal conductivity and dynamic viscosity of nanofluids," Energy Convers. Manag., vol. 52, no. 1, pp. 789–793, 2011.

[17] T. Yousefi, F. Veysi, E. Shojaeizadeh, and S. Zinadini, "An experimental investigation on the effect of Al_2O_3–H_2O nanofluid on the efficiency of flat-plate solar collectors," Renew. Energy, vol. 39, no. 1, pp. 293–298, 2012.

[18] Z. Said, M. H. Sajid, R. Saidur, M. Kamalisarvestani, and N. A. Rahim, "Radiative properties of nanofluids," Int. Commun. Heat Mass Transfer, vol. 46, pp. 74–84, 2013.

[19] S. K. Verma, A. K. Tiwari, and D. S. Chauhan, "Experimental evaluation of flat plate solar collector using nanofluids," Energy Convers. Manag., vol. 134, pp. 103–115, 2017.

[20] L. S. Sundar, M. K. Singh, and A. C. M. Sousa, "Enhanced heat transfer and friction factor of MWCNT–Fe_3O_4/water hybrid nanofluids," Int. Commun. Heat Mass Transfer, vol. 52, pp. 73–83, 2014.

ISSN (Online)
3048-8427
Vol. 3 | Issue 3
2026

[21] S. Choudhary, A. Sachdeva, and P. Kumar, "Investigation of the stability of MgO nanofluid and its effect on the thermal performance of flat plate solar collector," Renew. Energy, vol. 147, pp. 1801–1814, 2020.

[22] J. J. Michael and S. Iniyan, "Performance analysis of a copper sheet laminated photovoltaic thermal collector using copper oxide–water nanofluid," Sol. Energy, vol. 119, pp. 439–451, 2015.

[23] K. Farhana et al., "Improvement in the performance of solar collectors with nanofluids: A state-of-the-art review," Nano-Struct. Nano-Objects, vol. 18, art. 100276, 2019.

[24] A. M. Genc, M. A. Ezan, and A. Turgut, "Thermal performance of a nanofluid-based flat plate solar collector: A transient numerical study," Appl. Therm. Eng., vol. 130, pp. 395–407, 2018.

[25] V. Bianco, F. Scarpa, and L. A. Tagliafico, "Numerical analysis of the Al_2O_3–water nanofluid forced laminar convection in a flat plate solar collector," Renew. Energy, vol. 116, pp. 9–21, 2018.

[26] Y. Tong, J. Kim, and H. Cho, "Effects of thermal performance of enclosed-type evacuated U-tube solar collector with hybrid nanofluid," Renew. Energy, vol. 83, pp. 463–473, 2015.

[27] M. Moravej et al., "Enhancing the efficiency of a symmetric flat-plate solar collector via the use of rutile TiO_2–water nanofluids," Sustain. Energy Technol. Assessments, vol. 40, art. 100783, 2020.

[28] A. A. Hawwash, A. K. Abdel Rahman, S. A. Nada, and S. Ookawara, "Numerical investigation and experimental verification of performance enhancement of flat plate solar collector using nanofluids," Appl. Therm. Eng., vol. 130, pp. 363–374, 2018.

[29] Z. Said, M. E. H. Assad, A. A. Hachicha, E. Bellos, M. A. Abdelkareem, and D. Z. Alazzam, "Enhancing the performance of automotive radiators using nanofluids," Renew. Sustain. Energy Rev., vol. 112, pp. 183–194, 2019.

[30] A. H. Elsheikh, S. W. Sharshir, M. E. Mostafa, F. A. Essa, and M. K. A. Ali, "Applications of nanofluids in solar energy: A review of recent advances," Renew. Sustain. Energy Rev., vol. 82, pp. 3483–3502, 2018.

[31] A. K. Hamzat, M. I. Sahin, O. E. Omisanya, and A. Z. Sahin, "Application of nanofluid in solar energy harvesting devices: A comprehensive review," Energy Convers. Manag., vol. 266, art. 115790, 2022.

[32] E. Bellos and C. Tzivanidis, "A review of concentrating solar thermal collectors with and without nanofluids," J. Therm. Anal. Calorim., vol. 135, pp. 763–786, 2019.

[33] M. A. Sharafeldin and G. Gróf, "Efficiency of evacuated tube solar collector using WO_3/water nanofluid," Renew. Energy, vol. 134, pp. 453–460, 2019.

[34] O. A. Hussein et al., "Thermal performance enhancement of a flat plate solar collector using hybrid nanofluid," Sol. Energy, vol. 204, pp. 208–222, 2020.

[35] N. Akram et al., "A comprehensive review on nanofluid operated solar flat plate collectors," J. Therm. Anal. Calorim., vol. 139, pp. 1309–1343, 2020.

[36] E. Bellos, C. Tzivanidis, and Z. Said, "A systematic parametric thermal analysis of nanofluid-based parabolic trough solar collectors," Sustain. Energy Technol. Assessments, vol. 39, art. 100714, 2020.

[37] M. Sheikholeslami, M. Jafaryar, and Z. Li, "Nanofluid turbulent convective flow in a circular duct with helical turbulators considering CuO nanoparticles," Int. J. Heat Mass Transfer, vol. 124, pp. 980–989, 2018.

[38] R. Nasrin and M. A. Alim, "Semi-empirical relation for forced convective analysis through a solar collector," Sol. Energy, vol. 105, pp. 455–467, 2014.

[39] M. Faizal, R. Saidur, S. Mekhilef, and M. A. Alim, "Energy, economic and environmental analysis of metal oxides nanofluid for flat-plate solar collector," Energy Convers. Manag., vol. 76, pp. 162–168, 2013.

[40] M. Raissi, P. Perdikaris, and G. E. Karniadakis, "Physics-informed neural networks: A deep learning framework for solving forward and inverse problems involving nonlinear partial differential equations," J. Comput. Phys., vol. 378, pp. 686–707, 2019.

doi.org/10.5281/zenodo.21812228

ISSN (Online)
3048-8427
Vol. 3 | Issue 3
2026

[41] S. Cai, Z. Wang, S. Wang, P. Perdikaris, and G. E. Karniadakis, "Physics-informed neural networks for heat transfer problems," J. Heat Transfer, vol. 143, no. 6, art. 060801, 2021.

[42] E. Bellos and C. Tzivanidis, "Thermal analysis of parabolic trough collector operating with mono and hybrid nanofluids," Sustain. Energy Technol. Assessments, vol. 26, pp. 105–115, 2018.